# Structure to Property Relationships for Multiphoton Absorption in Covalently Linked Porphyrin Dimers: A Correction Vector INDO/MRDCI Study

**Lingyun Zhu,[†] Yuanping Yi,[†] Zhigang Shuai,*[,†] Karin Schmidt,[‡] and Egbert Zojer[§]**

*Key Laboratory of Organic Solids, Institute of Chemistry, Chinese Academy of Sciences, 100080 Beijing, P. R. China, Georgia Institute of Technology, School of Chemistry and Biochemistry, Atlanta, Georgia 30332-0400, Institute of Solid State Physics, Graz University of Technology, Petersgasse 16, A-8010 Graz, Austria*

*Received: April 5, 2007; In Final Form: June 29, 2007*

The correction vector method has been used to investigate structure to property relationships for multiphoton absorption properties in covalently linked porphyrin dimers. The electronic structure of the system is described within the multireference single and double configuration interaction (MRDCI) method coupled with the intermediate neglect of differential overlap (INDO) Hamiltonian. We find a strong increase in the two-photon absorption (2PA) and three-photon absorption (3PA) cross sections when going from an isolated porphyrin to the dimers. The nature of the 2PA and 3PA active states as well as the cross sections show a strong but not straightforward dependence on the length of the bridge between the two porphyrins. Our theoretical results are in very good agreement with experimental data for 2PA. The resulting structure to property relationships are analyzed on the basis of essential-state models, where it turns out that a three-state model considering only the $Q_x$ intermediate state proposed in literature does not provide a full description of the actual situation.

## I. Introduction

Multiphoton absorption processes are highly promising for a number of processes including optical limiting,[1] 3D microfabrication,[2] and optical data storage.[3] More recently, various porphyrin systems have received particular attention in the context of multiphoton absorption[4−12] because of their large $\pi$ electron delocalization, flat structure, and high thermal stability. At the same time, they have been commonly accepted as tumor markers and photosensitizers in photodynamic therapy of cancer (PDT)[13] for decades and also they can be applied in various photochemical processes that are promising for optical memory and microfabrication.[14] For example, fused diporphyrin,[5] butadiyne linked-self-assembled porphyrins,[4] conjugation length extended porphyrin,[6,12] and aggregated porphyrins[7] have been extensively investigated, and the reported two-photon absorption cross sections ($\sigma_2$) in these range from 100 to 15 000 GM.

Recently, Drobizhev et al.[15] have found that: (1) a series of covalent bridge-linked porphyrin dimers possess extremely large $\sigma_2$, up to 10 000 GM in the near-IR, which is several hundred times larger than that obtained for the corresponding monomer in the same region; and (2) subtly changed $\pi$-conjugated bridges in the middle of dimers make a difference to $\sigma_2$ values. To better understand the nature of the strong enhancement in these porphyrin systems and the bridge effects in porphyrin dimers, we have implemented the correction vector (CV) method within the multireference single and double configuration interaction (MRDCI) method coupled with the intermediate neglect of differential overlap (INDO) Hamiltonian (MRDCI/INDO) to calculate linear absorption, two-photon absorption (2PA), as well as three-photon absorption (3PA) spectra for the porphyrin monomer and dimers. The structure to property relationships are also explained on the basis of essential-state models.

The most widely used theoretical methods involved in calculating the 2PA or 3PA cross sections ($\sigma_3$) are sum-over-states (SOS)[16] and response theory.[17] The SOS approaches involve a truncation in the summation over excited states with the actual number of considered states typically depending on the methodology. This is because that it is virtually impossible to obtain information on all excited states for molecules relevant for practical applications described at the necessary (highly correlated) level of theory. Such truncations may, however, lead to uncontrolled errors in the calculated optical coefficients.[18] The nonlinear response theory has been widely applied in nonlinear optical (NLO) properties and multiphoton absorption calculations.[19] However, it is usually done for a fixed frequency away from any resonant structure due to numerical convergence problems. Time-dependent density functional theory (TDDFT) has also been used to investigate 2PA properties by the Pachter[20] and Tretiak[21] groups. We note that, for third-order NLO properties, due to the self-interaction problems in DFT, the charges are always predicted to be much more delocalized than reality, which results in a much amplified third-order polarizability. Developing a better functional to correct such errors is a current challenge in DFT.[22]

The CV method[23] for the computation of general dynamic NLO coefficients is convergent for the full frequency range relevant for multiphoton absorption. The advantage of CV is that one needs only ground-state properties such as energy, wave function, and dipole moment. It gives exactly the same results as if one sums over all the excited states. We have successfully employed the CV method within the MRDCI or the coupled-cluster approximation coupled with either the INDO or the ab initio Hamiltonian to study multiphoton absorption properties.[24] It has been shown that the full spectra of 2PA and 3PA can be obtained.

* Corresponding author. E-mail: zgshuai@iccas.ac.cn.
[†] Key Laboratory of Organic Solids, Institute of Chemistry.
[‡] Georgia Institute of Technology, School of Chemistry and Biochemistry.
[§] Institute of Solid State Physics, Graz University of Technology.

10.1021/jp072670y CCC: $37.00 
Published on Web 08/04/2007

## II. Theoretical Methodologies

The chemical structures of the molecules studied in the present work are displayed in Figure 1. The alkyl groups of the molecules studied in the experiments[15] are replaced by H atoms in the calculations. The ground-state geometries of all compounds are optimized at the DFT level with the hybrid B3LYP functional and the 6-31G* basis set for C, N, Si, and H and the LANL2DZ basis set for Zn, as implemented in the Gaussian-03 package.[25]

In the CV method,[23,24] the NLO coefficients can be obtained on the basis of only the ground-state eigenvalue, eigenvector, and permanent dipole moment. For the first-order polarizability $\alpha_{ij}(\omega)$, starting from the SOS expression, it can be expressed as

$$\begin{aligned}\alpha_{ij}(-\omega;\omega) &= \sum_R \left[\frac{\langle G|\overline{\mu_i}|R\rangle\langle R|\overline{\mu_j}|G\rangle}{E_R - E_G - \hbar\omega - i\Gamma} + \frac{\langle G|\overline{\mu_j}|R\rangle\langle R|\overline{\mu_i}|G\rangle}{E_R - E_G + \hbar\omega + i\Gamma}\right] \\ &= \left\langle G\left|\overline{\mu_i}\right| \frac{1}{H - E_G - \hbar\omega - i\Gamma}\left|\overline{\mu_j}\right|G\right\rangle + \left\langle G\left|\overline{\mu_j}\right| \frac{1}{H - E_G + \hbar\omega + i\Gamma}\left|\overline{\mu_i}\right|G\right\rangle \quad (1) \\ &= \langle\phi_i^{(1)}(-\omega)|\overline{\mu_j}|G\rangle + \langle\phi_j^{(1)}(\omega)|\overline{\mu_i}|G\rangle\end{aligned}$$

where $|\phi_i^{(1)}(\omega)\rangle$ and $|\phi_i^{(1)}(-\omega)\rangle$ are defined through the following first-order correction vectors equation:

$$(H - E_G \pm \hbar\omega \pm i\Gamma_1)|\phi_i^{(1)}(\pm\omega)\rangle = \overline{\mu_i}|G\rangle \quad (2)$$

Here, $H$ is the CI Hamiltonian; $E_G$ is the ground-state energy, $\omega$ is the fundamental input frequencies, and the $\overline{\mu_i}$ are the dipole displacement operators defined as:

$$\overline{\mu_i} = \widehat{\mu_i} - \langle G|\widehat{\mu_i}|G\rangle \quad (3)$$

$\Gamma$ denotes a dampling factor (set to 0.1 eV in the calculations). The indices $i$ and $j$ are Cartesian coordinates. Equation 2 can be directly solved via a Davidson-like algorithm for the "monster" linear equation.[23,24]

To compute the third-order polarizability $\gamma_{ijkl}(-\omega;\omega,-\omega,\omega)$ and the fifth-order polarizability $\epsilon_{ijklmn}(-\omega;\omega,\omega,-\omega,\omega,-\omega)$ necessary for describing 2PA and 3PA processes, the following equations for the second-order correction vector $\phi_{ij}^{(2)}(\omega_1,\omega_2)$ and the third-order correction vector $\phi_{ijk}^{(3)}(\omega_1,\omega_2,\omega_3)$ have to be solved:

$$(H - E_G + \hbar\omega_2 + i\Gamma)|\phi_{ij}^{(2)}(\omega_1,\omega_2)\rangle = \overline{\mu_j}|\phi_i^{(1)}(\omega_1)\rangle \quad (4)$$

$$(H - E_G + \hbar\omega_3 + i\Gamma)|\phi_{ijk}^{(3)}(\omega_1,\omega_2,\omega_3)\rangle = \overline{\mu_k}|\phi_{ij}^{(2)}(\omega_1,\omega_2)\rangle \quad (5)$$

Finding the solution to eqs 4 and 5 is analogous to solving eq 2; $\gamma_{ijkl}(-\omega;\omega,-\omega,\omega)$ and $\epsilon_{ijklmn}(-\omega;\omega,\omega,-\omega,\omega,-\omega)$ can then be written in terms of the second-order ($\phi_{ij}^{(2)}(\omega_1,\omega_2)$) and third-order correction vector ($\phi_{ijk}^{(3)}(\omega_1,\omega_2,\omega_3)$) as:

$$\gamma_{ijkl}(-\omega;\omega,-\omega,\omega) = P_{ijkl}\langle\phi_i^{(1)}(-\omega)|\overline{\mu_j}|\phi_{kl}^{(2)}(-2\omega,-\omega)\rangle \quad (6)$$

$$\epsilon_{ijklmn}(-\omega;\omega,\omega,-\omega,\omega,-\omega) = P_{ijklmn}\langle\phi_{ij}^{(2)}(-2\omega,-\omega)|\overline{\mu_k}|\phi_{lmn}^{(3)}(-3\omega,-2\omega,-\omega)\rangle \quad (7)$$

The orientationally averaged $\alpha_{av}$ and $\gamma_{av}$ values are defined as:[23]

$$\alpha_{av} = \sum_{i=x,y,z}\frac{1}{3}\alpha_{ii} \quad (8)$$

$$\gamma_{av} = \sum_{i,j=x,y,z}\frac{1}{15}(2\gamma_{iijj} + \gamma_{ijji}) \quad (9)$$

For the molecules studied here, the contribution of $z$-components can be neglected (the $x$-axis is defined as connecting the two central Zn atoms, the $y$-axis is perpendicular to the $x$-axis, and the $xy$ plane is parallel to one of the porphyrin planes). As $\gamma_{xxyy} = \gamma_{xyyx}$ and $\gamma_{yyxx} = \gamma_{yxxy}$, the orientationally averaged $\gamma_{av}$ can be written as:

$$\gamma_{av} = \frac{1}{5}(\gamma_{xxxx} + \gamma_{yyyy} + \gamma_{xxyy} + \gamma_{yyxx}) \quad (10)$$

As pointed out by Cronstrand et al.,[19] the numerical calculation for the orientationally averaged fifth-order polarizability, $\epsilon_{av}$, is a formidable task. We have tested the influence of the $\epsilon_{yyyyyy}$ component on the 3PA cross section. We find that it does not play any appreciable role for the porphyrin dimers, and thus we will focus only on the $\epsilon_{xxxxxx}$ component.

The 1PA, 2PA, and 3PA cross sections, $\sigma_1$, $\sigma_2$, and $\sigma_3$, can finally be derived from the imaginary parts of orientationally averaged $\alpha_{av}$ and $\gamma_{av}$ and $\epsilon_{xxxxxx}$. They can be expressed as:

$$\sigma_1 = \frac{4\pi(\hbar\omega)L^2}{nc\hbar}\,\mathrm{Im}\,\alpha_{av} \quad (11)$$

$$\sigma_2 = \frac{4\pi^2(\hbar\omega)^2L^4}{n^2c^2\hbar}\,\mathrm{Im}\,\gamma_{av} \quad (12)$$

$$\sigma_3 = \frac{4\pi^3(\hbar\omega)^3L^6}{3n^3c^3\hbar}\,\mathrm{Im}\,\epsilon_{xxxxxx} \quad (13)$$

In this contribution, we have used the MRDCI[26] method with the semiempirical INDO[27] Hamiltonian linked to the CV method to study the one-, two-, and three-photon absorption properties of porphyrin derivatives. The Mataga−Nishimoto potential[28] is used to describe the Coulomb repulsion terms. (Parametrizing the Si atom in INDO is probably inappropriate. But from the first-principles DFT calculation for yPy, we find that Si (at the end cap of yPy) does not participate in the active Kohn−Sham orbitals, thus Si's contribution is very minor (see Table S1 in Supporting Information)). Details regarding the choice of the CI-active space and the reference determinants in the INDO/MRDCI procedure are available in the Supporting Information. In general, we have paid particular attention to choosing a consistent CI-active space and reference set for all studied molecules. Therefore, we have extensively tested effects related to varying the CI space and the number of reference determinants. Because of the large size of the investigated molecules, previously applied approaches including only between 2 (ref 29) and 6 (ref 30) orbitals for multiple excitations could not be applicable here. Therefore, we have extended the capabilities of the ZINDO code by making use of iterative diagonalization schemes. In this work, the CI active spaces consist of up to 12 occupied and 12 unoccupied molecular orbitals, corresponding to more than 300 000 configurations.

## III. Results and Discussion

**A. Molecular Structures.** The DFT geometry optimizations show that, in the monomer (compound yPy in Figure 1), the

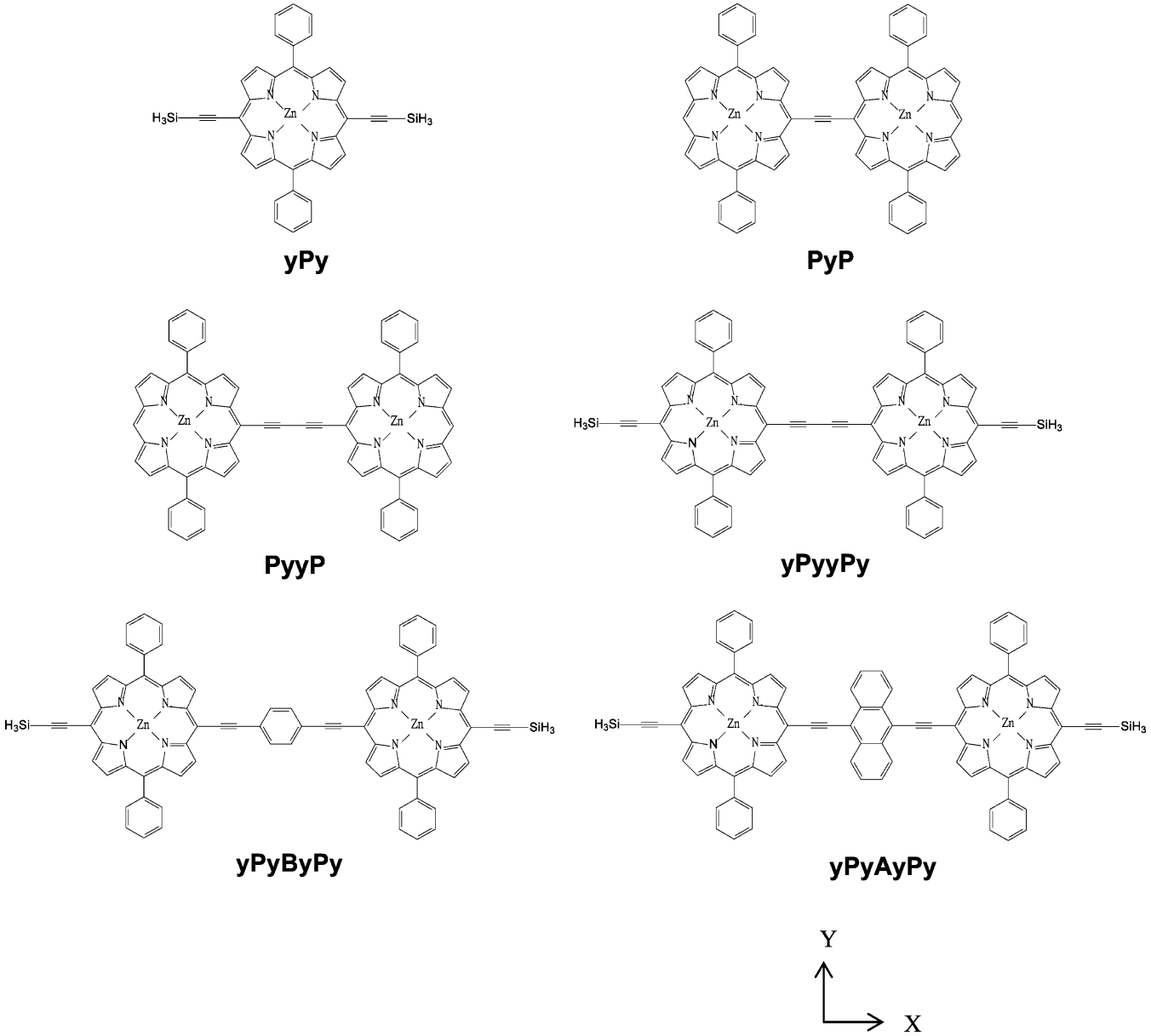


**Figure 1.** Chemical structures of the investigated porphyrin derivatives. The *XYZ* reference system is also shown.

porphyrin ring is planar and there is a twist of about 70° between the plane of the phenyl ring and that of the porphyrin. When having a single carbon−carbon triple bond bridging the gap between two porphyrin rings (compound PyP), the steric interaction between the closely neighboring $\beta$-hydrogens of the porphyrin rings distorts the molecule from planarity,[15b,31] resulting in a dihedral angle of ca. 36° between the porphyrins. This is in very good agreement with experimental and other DFT optimized results.[32] However, by adding another carbon−carbon triple bond between the two rings to form the PyyP and yPyyPy dimers, the minimum structures for the porphyrin rings are coplanar again. This increases the conjugation length and should make the backbone more polarizable. Also when an additional benzene ring is inserted into the middle of the two triple bonds of yPyyPy, the molecule yPyByPy remains coplanar. However, when the benzene ring is replaced by an anthracene, steric interactions again become stronger and the plane of the anthracene moiety is twisted by ca. 32° in yPyAyPy. The DFT optimized results for yPyyPy and yPyByPy dimers are in agreement with X-ray investigations.[33]

**B. One-Photon Absorption.** *i. yPy Monomer.* Figure 2a presents the MRDCI/CV calculated one-photon absorption spectrum of the yPy monomer. We find that the linear absorption spectrum in the low-energy region is dominated by a very weak $Q_x$ band at ca. 2.07 eV. There is another very weak band ($Q_y$) at ca. 1.95 eV, whose oscillator strength is about one-fifth of the main $Q_x$ band. The authors of ref 15 attribute the lowest band at ca. 1.9 eV (646 nm) to a $Q_y$ band and the other very weak band at about 2.1 eV (595 nm) to $Q_x$. The calculated transition energies agree well with the experimental polarized absorption spectrum in the low-energy region.[15] (The slight overestimation of calculated excitation energies is attributed to an overcorrelation of the ground state[34] in the MRDCI method.) However, the assignment of the polarization of these two bands is reversed between our study and the previous studies. This is because the assignment in ref 15 is based on calculations[35] for the molecule ($Zn_1-(T)_2$ and $Zn_1-(TT)_2$, where R2 are H atoms) that is different from our studied yPy molecule (R2 phenyl rings). (To verify our theoretical results, we have performed INDO/SCI calculations on the yPy molecule and the $Zn_1-(T)_2$

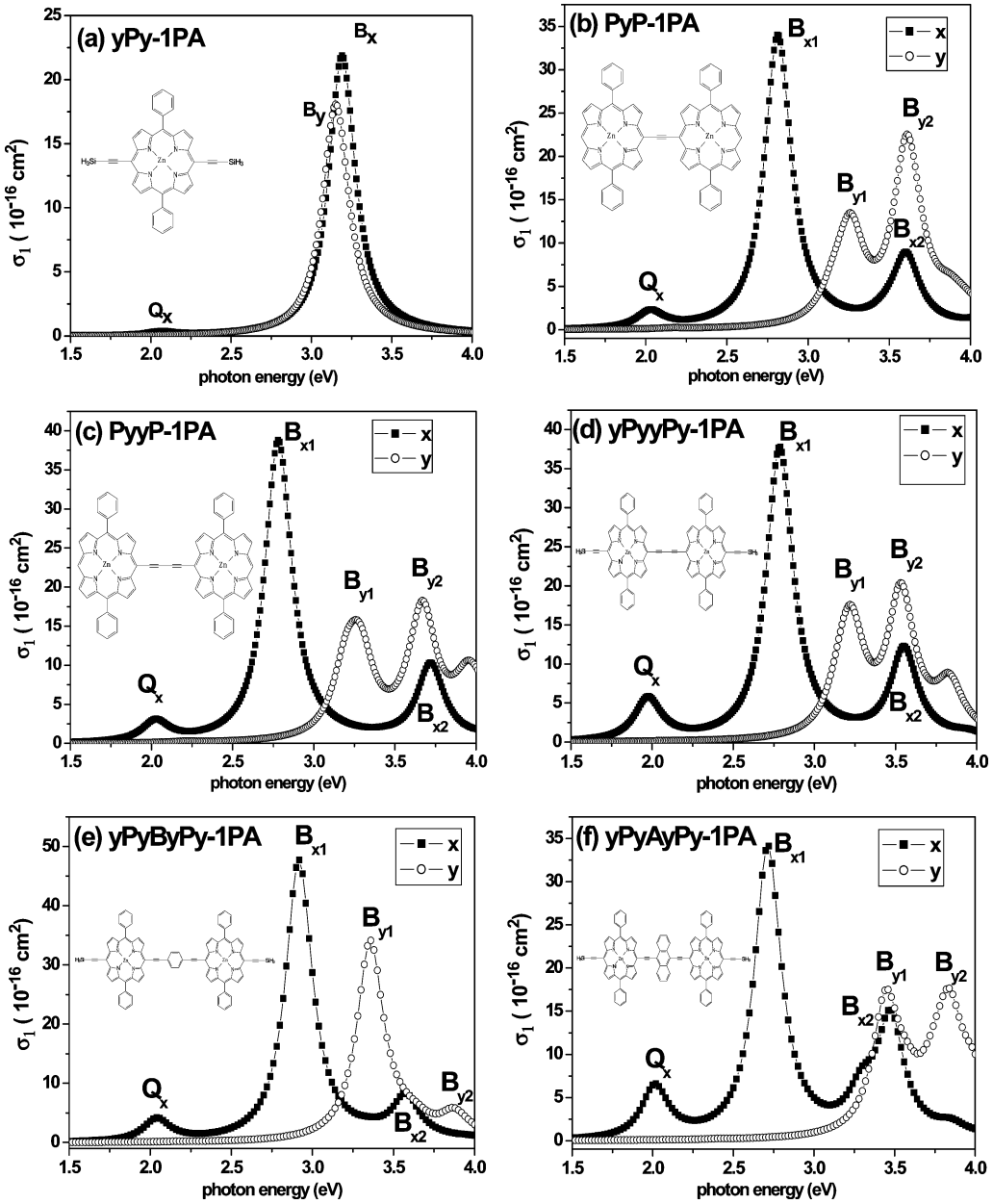


**Figure 2.** MRDCI/CV calculated *x*-,*y*-polarized one-photon absorption spectra of the molecules shown in Figure 1.

and $Zn_1-(TT)_2$ molecules in ref 35. For yPy, INDO/SCI calculated results are consistent with our INDO/MRDCI result and show that the oscillator strength of $Q_x$ is larger than that of $Q_y$; for $Zn_1-(T)_2$ and $Zn_1-(TT)_2$ monomers, the oscillator strength of $Q_y$ is larger than $Q_x$, which is in agreement with the calculation results in ref 35; see Table S9 in the Supporting Information.)

In the high-energy region of the linear absorption spectrum, there are two close-lying strong B-bands, $B_y$ and $B_x$, peaking at ca. 3.15 and 3.19 eV, respectively. The energetic splitting of the $B_x$ and $B_y$ bands is 0.04 eV, which is somewhat smaller than the experimental splitting ($B_x$ at 2.73 eV and $B_y$ at 2.81 eV).[15] When using the above-described (presumably inappropriate) assignment of *x*- and *y*-polarized components in ref 15, the relative oscillator strengths of $B_x$ and $B_y$ would again be reversed between theory and experiment.

*ii. Porphyrin Dimers.* The MRDCI/CV simulated linear absorption spectra of a series of porphyrin dimers are shown in Figure 2b−f. For *x*-polarized light, all porphyrin dimers show common trends when compared to the monomer: (a) The oscillator strengths associated with the $Q_x$ bands are drastically enhanced and the peaks are red-shifted, a feature that arises from partial wave function delocalization between the two porphyrins and the benzene or anthracene units. (b) The $B_x$ bands split into two sub-bands; $B_{x1}$ lies between ca. 2.7 and 2.9 eV and $B_{x2}$ is found around 3.5−3.7 eV (see Table 1). These results are in good agreement with the experimental trends,[15] which also show that the lowest-energy Q-band is strongly intensified and red-shifted, while the B band splits into several sub-bands. (c) The oscillator strengths of $B_{x1}$ are always larger than of $B_{x2}$. In the experiments, however, the oscillator strength of $B_{x1}$ and $B_{x2}$ is similar in yPyyPy and the intensity ratio is inverted in yPyByPy and yPyAyPy. To test whether this discrepancy results from the limited CI space in the MRDCI calculations, we have also done a SCI calculation with much bigger CI-active spaces (including the highest 70 occupied and the lowest 70 unoccupied orbitals) for yPyByPy and yPyAyPy, but also there we find the oscillator strength associated with $B_{x1}$ always larger than for $B_{x2}$.

**TABLE 1: MRDCI/CV and Tensor Method Calculated One-, Two-, and Three-Photon Absorption Properties of Porphyrin Derivatives[a]**

| | 1PA | | | 2PA | | | | | | 3PA | | | |
|---|---|---|---|---|---|---|---|---|---|---|---|---|---|
| | CV | | | CV | | tensor | | exp | | CV | | tensor | |
| compound | $Q_x$ (eV) | $B_x$ (eV) | $B_y$ (eV) | peak (eV) | $\sigma_2$ | peak (eV) | $\sigma_2$ | peak (eV) | $\sigma_2$ | peak (eV) | $\sigma_{3(xxxxxx)}$ | peak (eV) | $\sigma_{3(xxxxxx)}$ |
| YPy | 2.07 | 3.19 | 3.15 | 1.52 | 46 | 1.52 | 25 | | | 0.70 | 0.01 | 0.70 | 0.01 |
| | | | | 1.89 | 406 | 1.91 | 262 | 1.46 | 20 | 1.08 | 0.16 | 1.08 | 0.1 |
| PyP | 2.03 | 2.81 | 3.26 | 1.48 | 1755 | 1.48 | 1692 | | | 0.94 | 65 | 0.94 | 14 |
| | | 3.60 | 3.61 | 1.85 | 8022 | 1.86 | 7098 | 1.50 | 8600 | 1.21 | 2043 | 1.21 | 2450 |
| PyyP | 2.03 | 2.78 | 3.26 | 1.46 | 2175 | 1.46 | 1986 | | | 0.93 | 162 | 0.94 | 49 |
| | | 3.72 | 3.67 | 1.86 | 19473 | 1.88 | 20549 | 1.48 | 5500 | 1.25 | 5605 | 1.25 | 6440 |
| YPyyPy | 1.98 | 2.79 | 3.22 | 1.38 | 2205 | 1.39 | 1957 | | | 0.94 | 312 | 0.94 | 147 |
| | | 3.55 | 3.53 | 1.79 | 28655 | 1.81 | 31511 | 1.40 | 9100 | 1.19 | 6972 | 1.19 | 9030 |
| YPyByPy | 2.04 | 2.92 | 3.36 | 1.55 | 2874 | 1.56 | 2550 | | | 0.98 | 252 | 0.98 | 70 |
| | | 3.58 | 3.86 | 1.81 | 12188 | 1.80 | 9228 | 1.41 | 3800 | 1.20 | 4212 | 1.20 | 4130 |
| YPyAyPy | 2.02 | 2.72 | 3.46 | 1.46 | 3835 | 1.46 | 3484 | 1.4 | 4000 | 0.91 | 308 | 0.92 | 112 |
| | | 3.48 | 3.84 | 1.76 | 16929 | 1.77 | 15141 | 1.47 | 10100 | 1.16 | 5060 | 1.17 | 5320 |

[a] Experimental 2PA data[15] are also listed. Averaged 2PA cross section in the units of $10^{-50}$ cm$^4$ s (GM) and 3PA cross section of the xxxxxx component in the units of $10^{-80}$ cm$^6$ s$^2$.

**C. Two-Photon Absorption.** Figure 3 shows the MRDCI/CV calculated 2PA spectra of the investigated porphyrin derivatives. In parts a and b of Figure 3, filled squares, open circles, filled triangles, and open triangles show the contributions of the *xxxx*, *yyyy*, *xxyy*, and *yyxx* components of $\sigma_2$ of yPy and PyP, respectively. In Figure 3c, we report the averaged 2PA spectra (according to eq 12) for all porphyrin dimers. Table 1 gives the averaged $\sigma_2$ values of the porphyrin derivatives.

*i. yPy Monomer.* For the yPy monomer, there are two 2PA peaks (around 1.52 and 1.89 eV) in the spectral range below linear absorption (see Figure 3a). All four plotted components contribute to averaged signal; the *xxxx* component is dominant in the region of the low-energy peak, while the *yyyy* component is the strongest one at the high-energy peak. The first 2PA maximum is at a photon energy of 1.52 eV; the corresponding averaged $\sigma_2$ value at this energy is 46 GM. The second 2PA peak is located at 1.89 eV, which corresponds to the main experimental peak at 1.46 eV, because the photon energy of main 2PA peak is higher than that of the main linear absorption feature in the B-band region. The calculated averaged $\sigma_2$ of the second 2PA peak is 406 GM, which is overestimating the experimental value (20GM).

*ii. Porphyrin Dimers.* From Figure 3b, we find that the longitudinal *xxxx* component of the 2PA amplitude in PyP dimer is several orders of magnitude larger than that of any other tensor component. This can be understood from the increased conjugation along the *x*-axis connecting the two porphyrins.

From parts b and c of Figure 3, one can see that there typically is a double peak structure in the 2PA spectra, with a first peak around 1.5 eV and the high-energy main peak in the region around 1.8 eV. The latter typically has a low-energy shoulder around 1.7 eV. Such a double peak structure is also resolved in several of the experimental spectra, in particular in PyyP and very strongly in yPyAyPy. Both, in the experiments and in the calculations, the lower-energy peak is in the energy region of the lower $B_x$ band, while the higher peak is at a photon energy higher than the main linear absorption feature in the B-band region.

In this context, it should be mentioned that, for centrosymmetric molecules, 2PA states are different from one-photon states due to mutually exclusive selection rules. Thus, while the molecules investigated here have 2PA states that are in the region of certain strongly one-photon active states, they differ from those in their wave function symmetry. For example, in the PyP dimer, the low-energy 2PA state (at $1.48 \times 2 = 2.96$ eV) corresponds to the $S_6$ excited state, whose description is dominated by a determinant with an electron excited from the HOMO to the LUMO+3 molecular orbital. The corresponding one-photon state (2.81 eV) corresponds to the $S_5$ excited state, dominated by a transition from the HOMO to the LUMO orbital. It is found that LUMO ($B_g$) and LUMO+3 ($A_u$) orbitals have inverse symmetry, the HOMO has $A_u$ symmetry. That testifies to our results that $S_6$ is a two-photon allowed excited-state and $S_5$ is a one-photon allowed but two-photon forbidden excited state.

Several trends can be seen in the calculated spectra: (a) It is noted that, in the experiment, the 2PA peaks of the monomer and the dimers are in similar photon energy ranges. So in the calculation, we should also compare the high-energy 2PA peak of the monomer with the high-energy 2PA peak of the dimers. When going from the monomer, yPy (with $\sigma_2 = 406$ GM at 1.89 eV) to the dimer, yPyyPy, (with $\sigma_2 = 28.7 \times 10^3$ GM at 1.79 eV), there is a nearly 2 orders of magnitude increase in $\sigma_2$. This is fully consistent with the experimental trend (there is ~400-fold enhancement in the dimer as compared to the parent monomer), although in the calculations, the $\sigma_2$ value is more strongly overestimated for the monomer ($\sigma_2 = 20$ GM at 1.46 eV in the experiment) than for the dimer($\sigma_2 = 9100$ GM at 1.40 V in the experiment). (b) Looking at PyyP, yPyyPy, and yPyByPy, the experimental and theoretical trends are consistent: there is a strong increase in $\sigma_2$ (nearly doubling) when going from PyyP ($19.5 \times 10^3$ GM at 1.86 eV) to yPyyPy ($28.7 \times 10^3$ GM at 1.79 eV) both in theory and experiment and $\sigma_2$ decrease again in yPyByPy ($12.2 \times 10^3$ GM at 1.81 eV; in this molecule, the width of the experimental peak, however, seems to be significantly increased). Also the shift of the 2PA peak to lower energies when going from PyyP to yPyyPy and back to a higher energy intermediate between the two in yPyByPy is consistent between experiments and calculations. (c) The absolute values of the cross sections of the strong peaks in PyyP, yPyyPy, and yPyByPy are, however, significantly overestimated by the calculations, while for PyP and yPyAyPy, also the absolute magnitudes in the calculations agree well with those in the experiment.[36] This observation is insofar intriguing, as only for PyP and yPyAyPy have steric interactions been found to induce a twist between the planes of the two porphyrins. The

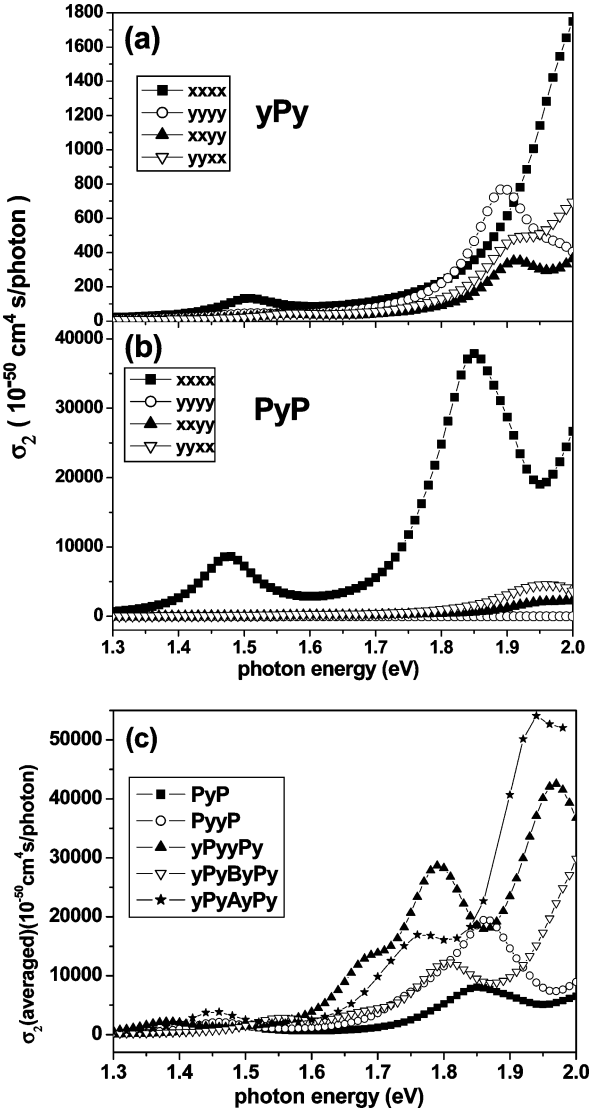


**Figure 3.** MRDCI/CV calculated two-photon absorption spectra. (a) and (b): filled squares, open circles, filled triangles and open triangles show the contributions of the *xxxx*, *yyyy*, *xxyy*, and *yyxx* components of the two-photon absorption cross section, respectively, for the yPy monomer and the PyP dimer; (c) are the orientationally averaged 2PA spectra for all porphyrin dimers.

reduced conjugation resulting from that twist can then be held responsible for the comparably smaller calculated $\sigma_2$ in PyP and yPyAyPy. In the other dimers, there is no steric inhibition to a free rotation around the axis connecting the two porphyrins. This might imply that in the experiments on PyyP, yPyyPy, and yPyByPy in solution, one is dealing not only with planar molecules as assumed here (based on the geometry optimizations neglecting the interaction with the solvent). The reduced conjugation in twisted conformers could then be responsible for the measured "average" cross sections in those three materials being significantly smaller than the calculated one.[37]

To be able to analyze the results based on essential state models,[38] we have compared the CV results with S-tensor[39] calculations including 100 excited states. The 2PA cross section, $\sigma_2$ ($\omega$), can be expressed according the relationship

$$\sigma_2(\omega) = \frac{4\pi^2(\hbar\omega)^2 L^4}{n^2 c^2 \hbar} \sum_f \left| S^{ij}_{g\to f} \right|^2 \left\{ \frac{\Gamma}{(E_{gf} - 2\hbar\omega)^2 + \Gamma^2} \right\} \quad (14)$$

where $c$ is the speed of light in vacuum. $L$ denotes a local-filed correction (equal to 1 for vacuum), $\hbar\omega$ is the photon energy of the incident light, and $\Gamma$ is a Lorenzian broading factor (set to 0.1 eV in the calculations). $S_{g\to f}$ corresponds to the two-photon transition amplitude from the ground state to a final two-photon state $|f\rangle$, with the tensor $ij$ component defined as

$$S^{ij}_{g\to f} = \sum P_{ij} \sum_m \frac{\langle g|\mu_i|m\rangle\langle m|\mu_j|f\rangle}{E_{gm} - \hbar\omega - i\Gamma} \quad (15)$$

where $E_{gm}$ corresponds to the excitation energy from the ground state $|g\rangle$ to excited state $|m\rangle$, $\mu_i$ is the component of the electric dipole operator along the molecular axis $i$, and $P_{ij}$ denotes a complete permutation of the indices $i$ and $j$. For linearly polarized light, the average $\sigma_2$ can be written as[40]

$$\sigma_2(\omega) = \frac{4\pi^2(\hbar\omega)^2 L^4}{15 n^2 c^2 \hbar} \sum_f \left| \sum_{ij} S^{ii}_{g\to f} S^{ij\,*}_{g\to f} + 2\sum_{ij} S^{ij}_{g\to f} S^{ij\,*}_{g\to f} \right| \left\{ \frac{\Gamma}{(E_{gf} - 2\hbar\omega)^2 + \Gamma^2} \right\} \quad (16)$$

We find that the trends obtained for $\sigma_2$ with the two methods are consistent. Thus we have been able to analyze the dominant channels contributing to $|S_{g\to f}|^2 (E_{gf})^2\ \Gamma/\{(E_{gf} - 2\hbar\omega)^2 + \Gamma^2\}$. It consists of a sum of terms of the type $\mu^i_{ge}\mu^j_{ef}/\{E_{ge} - 1/2\ E_{gf}\}$, where the numerator contains the transition dipoles between the ground state an the intermediate state (over which the summation occurs) and the intermediate state and the 2PA active state; the denominator is given by the detuning energy of the respective intermediate state. $\Gamma$ is a broadening factor, $\hbar\omega$ is the photon energy at the 2PA peak, and $E_{gf}$ is the transition energy from the ground state to the 2PA final state.

Calculating $S_{g\to f}$ then allows identifying the most important intermediate excited states. In Tables 2 and 3, the dominant channels of the perturbative S-tensor description for 2PA into the main high-energy peak and into low-energy peak are listed. Channels, in which the $Q_x$, $B_{x1}$, and $B_{x2}$ states serve as intermediate states, have been found to give rise to the largest relative contribution to the overall $\sigma_2$ because they possess large $\mu_{ge}$ and, in case of dimers, also large $\mu_{ef}$ (listed in Tables 2 and 3). Considering these one-photon states for $|S_{g\to f}|^2$ gives rise to the following: (i) channels involving only the one-photon state $Q_x$, (ii) channels containing only one type of $B_i$ ($i = x_1$ or $x_2$) intermediate states, and (iii) mixed channels.[38e,41] In the following, they will be referred to as MN channels (with M and N being either Q, $B_{x1}$, or $B_{x2}$). Note that the sign of $\mu_{ge}\cdot\mu_{ef}$ into $B_{x2}$ is reversed with respect to $\mu_{ge}\cdot\mu_{ef}$ into $B_{x1}$ and Q for all the dimers (see column 6 and 7 in Table 2). Thus, all channels that involve $B_{x2}$ in combination with either Q or $B_{x1}$ ($QB_{x2}$ and $B_{x1}B_{x2}$ channels, see column 11 and 14 in Table 2) as intermediate states lead to negative contributions to $\sigma_2$.

This analysis provides the following insights: (a) A nearly 2 orders of magnitude increase when going from yPy to the corresponding dimer yPyyPy can then be explained on the basis of individual transition dipoles as well as the detuning energy. As far as the B-channels are concerned, they are strongly enhanced due to the increase of $\mu_{ge}$ and much more importantly $\mu_{ef}$. The decrease of the detuning energies ($E_{ge} - E_{ef}/2$) results in a further increased cross section. In yPyyPy, we also observe a much larger contribution from Q-channels (see ratio $(QQ + QB_{x1})/(B_{x1}B_{x1})$ as seen in the values in Table 2, which is due to the much smaller detuning energies. (b) When considering the combined solely $B_{xi}$-based channels ($i = 1,2$) as BB contribution

**TABLE 2: Dominant Excited States That Contribute to 2PA into the Main High-Energy Peak[a]**

| compound | final state | intermediate state | $E_{ge}$ | $E_{gf}$ | $\mu_{ge}$ | $\mu_{ef}$ | detuning energy | QQ | $QB_{x1}$ | $QB_{x2}$ | $B_{x1}B_{x1}$ | $B_{x2}B_{x2}$ | $B_{x1}B_{x2}$ |
|---|---|---|---|---|---|---|---|---|---|---|---|---|---|
| yPy | $S_9$ | $S_5$ ($B_y$) | 3.15 | 3.78 | 12.02($\mu^y$) | 4.47($\mu^y$) | 1.26 | | | | | | |
| | | $S_6$ ($B_x$) | 3.19 | 3.78 | −13.15 | 2.23 | 1.30 | | | | | | |
| | | $S_2$ ($Q_x$) | 2.06 | 3.78 | 1.84 | 2.94 | 0.17 | | | | | | |
| | $S_{10}$ | $S_5$ ($B_y$) | 3.15 | 3.82 | 12.02($\mu^y$) | 1.29 | 1.24 | | | | | | |
| | | $S_6$ ($B_x$) | 3.19 | 3.82 | −13.15 | −1.44 | 1.28 | | | | | | |
| | | $S_2$ ($Q_x$) | 2.06 | 3.82 | 1.84 | 2.11 | 0.15 | | | | | | |
| PyP | $S_{25}$ | $S_1$ ($Q_x$) | 2.03 | 3.69 | 4.90 | −6.57 | 0.19 | | | | | | |
| | | $S_5$ ($B_{x1}$) | 2.81 | 3.69 | −17.43 | 9.07 | 0.97 | 0.37 | 0.69 | −0.21 | 0.32 | 0.03 | −0.20 |
| | | $S_{19}$ ($B_{x2}$) | 3.6 | 3.69 | −7.44 | −11.77 | 1.76 | | | | | | |
| | $S_{26}$ | $S_1$ ($Q_x$) | 2.03 | 3.81 | 4.90 | 3.93 | 0.13 | | | | | | |
| | | $S_5$ ($B_{x1}$) | 2.81 | 3.81 | −17.43 | −4.53 | 0.91 | 0.53 | 0.60 | −0.21 | 0.17 | 0.02 | −0.11 |
| | | $S_{19}$ ($B_{x2}$) | 3.6 | 3.81 | −7.44 | 6.91 | 1.70 | | | | | | |
| | $S_{18}$ | $S_1$ ($Q_x$) | 2.03 | 3.59 | 4.90 | 3.27 | 0.24 | | | | | | |
| | | $S_5$ ($B_{x1}$) | 2.81 | 3.59 | −17.43 | −5.56 | 1.02 | 0.25 | 0.71 | −0.21 | 0.50 | 0.04 | −0.29 |
| | | $S_{19}$ ($B_{x2}$) | 3.6 | 3.59 | −7.44 | 6.93 | 1.81 | | | | | | |
| PyyP | $S_{26}$ | $S_1$ ($Q_x$) | 2.02 | 3.73 | 5.71 | 9.03 | 0.16 | | | | | | |
| | | $S_5$ ($B_{x1}$) | 2.78 | 3.73 | 18.72 | 12.90 | 0.92 | 0.40 | 0.63 | −0.16 | 0.25 | 0.02 | −0.14 |
| | | $S_{25}$ ($B_{x2}$) | 3.72 | 3.73 | −8.01 | 15.63 | 1.86 | | | | | | |
| | $S_{17}$ | $S_1$ ($Q_x$) | 2.02 | 3.60 | 5.72 | 6.64 | 0.22 | | | | | | |
| | | $S_5$ ($B_{x1}$) | 2.78 | 3.60 | 18.72 | 6.09 | 0.98 | 0.43 | 0.57 | −0.12 | 0.19 | 0.01 | −0.08 |
| | | $S_{25}$ ($B_{x2}$) | 3.72 | 3.6 | −8.01 | 5.84 | 1.92 | | | | | | |
| yPyyPy | $S_{24}$ | $S_1$ ($Q_x$) | 1.97 | 3.62 | 8.31 | −6.90 | 0.16 | | | | | | |
| | | $S_6$ ($B_{x1}$) | 2.78 | 3.62 | −18.42 | 7.09 | 0.97 | 0.66 | 0.48 | −0.17 | 0.09 | 0.01 | −0.07 |
| | | $S_{22}$ ($B_{x2}$) | 3.55 | 3.62 | 8.92 | 9.13 | 1.74 | | | | | | |
| | $S_{23}$ | $S_1$ ($Q_x$) | 1.97 | 3.58 | 8.31 | 6.82 | 0.18 | | | | | | |
| | | $S_6$ ($B_{x1}$) | 2.78 | 3.58 | −18.42 | −9.02 | 0.99 | 0.55 | 0.58 | −0.20 | 0.16 | 0.02 | −0.11 |
| | | $S_{22}$ ($B_{x2}$) | 3.55 | 3.58 | 8.92 | −11.18 | 1.76 | | | | | | |
| | $S_{21}$ | $S_1$ ($Q_x$) | 1.97 | 3.55 | 8.31 | −6.57 | 0.20 | | | | | | |
| | | $S_6$ ($B_{x1}$) | 2.78 | 3.55 | −18.42 | 10.55 | 1.01 | 0.47 | 0.65 | −0.22 | 0.22 | 0.03 | −0.15 |
| | | $S_{22}$ ($B_{x2}$) | 3.55 | 3.55 | 8.92 | 12.98 | 1.78 | | | | | | |
| | $S_{13}$ | $S_1$($Q_x$) | 1.97 | 3.36 | 8.31 | −9.78 | 0.29 | | | | | | |
| | | $S_6$($B_{x1}$) | 2.78 | 3.36 | −18.42 | 9.40 | 1.10 | 0.50 | 0.56 | −0.14 | 0.16 | 0.01 | −0.09 |
| | | $S_{22}$ ($B_{x2}$) | 3.55 | 3.36 | 8.92 | 8.25 | 1.87 | | | | | | |
| yPyByPy | $S_{19}$ | $S_5$($B_{x1}$) | 2.92 | 3.60 | −20.27 | 13.89 | 1.12 | | | | | | |
| | | $S_{18}$($B_{x2}$) | 3.58 | 3.60 | 6.81 | 24.97 | 1.78 | 0.23 | 0.81 | −0.31 | 0.70 | 0.10 | −0.53 |
| | | $S_1$($Q_x$) | 2.04 | 3.60 | −6.80 | 5.07 | 0.24 | | | | | | |
| | $S_{17}$ | $S_5$($B_{x1}$) | 2.92 | 3.56 | −20.27 | 10.55 | 1.14 | | | | | | |
| | | $S_{18}$($B_{x2}$) | 3.58 | 3.56 | 6.81 | 19.63 | 1.8 | 0.18 | 0.81 | −0.32 | 0.91 | 0.14 | −0.72 |
| | | $S_1$($Q_x$) | 2.04 | 3.56 | −6.80 | 3.18 | 0.26 | | | | | | |
| yPyAyPy | $S_{12}$ | $S_1$($Q_x$) | 2.01 | 3.52 | 8.70 | −8.29 | 0.25 | | | | | | |
| | | $S_5$($B_{x1}$) | 2.71 | 3.52 | 17.72 | −10.50 | 0.95 | 0.48 | 0.66 | −0.24 | 0.22 | 0.03 | −0.15 |
| | | $S_{11}$($B_{x2}$) | 3.47 | 3.52 | 9.81 | 12.21 | 1.71 | | | | | | |
| | $S_8$ | $S_1$($Q_x$) | 2.01 | 3.42 | 8.70 | 5.93 | 0.30 | | | | | | |
| | | $S_5$($B_{x1}$) | 2.71 | 3.42 | 17.72 | 8.57 | 1.00 | 0.30 | 0.54 | −0.04 | 0.24 | 0.00 | −0.04 |
| | | $S_{11}$($B_{x2}$) | 3.47 | 3.42 | 9.81 | −2.03 | 1.76 | | | | | | |
| | $S_{15}$ | $S_1$($Q_x$) | 2.01 | 3.63 | 8.70 | 1.42 | 0.20 | | | | | | |
| | | $S_5$($B_{x1}$) | 2.71 | 3.63 | 17.72 | 10.38 | 0.90 | 0.14 | 0.92 | −0.45 | 1.49 | 0.35 | −1.45 |
| | | $S_{11}$($B_{x2}$) | 3.47 | 3.63 | 9.81 | −16.92 | 1.66 | | | | | | |

[a] Listed are the INDO/MRDCI calculated excitation energies (eV) of 2PA-active and intermediate states and transition dipoles (Debye); if not specified, the component along the *x*-direction of the transition dipole moment is quoted. For dimers, we also give the relative participations of resulting 2PA channels for the dimers; channels involving $Q_x$ as intermediate state are denoted as QQ, channels with $B_{xi}$ ($i = 1,2$) intermediate state as $B_{xi}B_{xi}$ channels and mixed channels with $Q_x$, $B_{x1}$, or $B_{x2}$ as one of the intermediated states as $QB_{xi}$ and $B_{x1}B_{x2}$ channels, respectively.

and the combined $QB_{x1}$ and $QB_{x2}$ channels as QB contribution, it becomes evident from Table 3 that the low-energy 2PA peak is dominated by QB, whose contribution is ca. 50% throughout the dimers. The remaining 50% are provided by BB and QQ channels, whose ratio can vary between 0.45 (PyP) and 1.7 (yPyyPy). (c) For the main high-energy peak (which is a superposition of 2PA into several excited states), we find that typically both Q- and B-based channels significantly contribute to the 2PA response. The former play a strong role due to the much smaller associated detuning energies, while the latter are strong because of the larger transition dipoles from the $B_x$ states both to the ground as well as to the 2PA states. The relative contributions vary significantly from molecule to molecule (see Table 2), which makes an analysis based on a three-state model with $Q_x$ as the intermediate state without considering $B_x$ states (as in ref 15) somewhat problematic.

The trends for the main peak of the dimers will first be discussed for the planar molecules (PyyP, yPyyPy, and yPy-

**TABLE 3: Dominant Excited States That Contribute to 2PA into the Main Low-Energy Peak[a]**

| compound | final state | intermediate state | $E_{ge}$ | $E_{gf}$ | $\mu_{ge}$ | $\mu_{ef}$ | detuning energy | QQ | $QB_{x1}$ | $QB_{x2}$ | $B_{x1}B_{x1}$ | $B_{x2}B_{x2}$ | $B_{x1}B_{x2}$ |
|---|---|---|---|---|---|---|---|---|---|---|---|---|---|
| yPy | $S_4$ | $S_6$ ($B_x$) | 3.19 | 3.13 | −13.15 | 1.85($\mu^y$) | 1.63 | | | | | | |
| | | $S_5$ ($B_y$) | 3.15 | 3.13 | 12.02($\mu^y$) | −1.97 | 1.59 | | | | | | |
| | | $S_2$ ($Q_x$) | 2.06 | 3.13 | 1.84 | 3.34($\mu^y$) | 0.50 | | | | | | |
| | $S_3$ | $S_6$ ($B_x$) | 3.19 | 3.01 | −13.15 | −1.38 | 1.69 | | | | | | |
| | | $S_5$ ($B_y$) | 3.15 | 3.01 | 12.02($\mu^y$) | −1.37($\mu^y$) | 1.65 | | | | | | |
| | | $S_2$ ($Q_x$) | 2.06 | 3.01 | 1.84 | 3.11 | 0.56 | | | | | | |
| PyP | $S_6$ | $S_5$ ($B_{x1}$) | 2.81 | 2.95 | −17.43 | −14.13 | 1.34 | | | | | | |
| | | $S_{19}$ ($B_{x2}$) | 3.60 | 2.95 | −7.44 | 23.07 | 2.13 | 0.19 | 0.87 | −0.38 | 1.01 | 0.19 | −0.88 |
| | | $S_1$ ($Q_x$) | 2.03 | 2.95 | 4.90 | 9.05 | 0.56 | | | | | | |
| PyyP | $S_6$ | $S_5$ ($B_{x1}$) | 2.78 | 2.91 | 18.72 | 13.92 | 1.33 | | | | | | |
| | | $S_{25}$ ($B_{x2}$) | 3.72 | 2.91 | −8.01 | 22.64 | 2.27 | 0.18 | 0.82 | −0.34 | 0.95 | 0.16 | −0.77 |
| | | $S_1$ ($Q_x$) | 2.02 | 2.91 | 5.72 | 8.41 | 0.57 | | | | | | |
| yPyyPy | $S_5$ | $S_6$ ($B_{x1}$) | 2.78 | 2.76 | −18.42 | −14.10 | 1.40 | | | | | | |
| | | $S_{22}$($B_{x2}$) | 3.55 | 2.76 | 8.92 | −23.05 | 2.17 | 0.32 | 1.00 | −0.51 | 0.78 | 0.20 | −0.79 |
| | | $S_1$ ($Q_x$) | 1.97 | 2.76 | 8.31 | 8.51 | 0.59 | | | | | | |
| yPyByPy | $S_6$ | $S_5$ ($B_{x1}$) | 2.92 | 3.10 | −20.27 | 14.47 | 1.37 | | | | | | |
| | | $S_{18}$ ($B_{x2}$) | 3.58 | 3.10 | 6.81 | 26.34 | 2.03 | 0.18 | 0.83 | −0.34 | 0.96 | 0.16 | −0.79 |
| | | $S_1$ ($Q_x$) | 2.04 | 3.10 | −6.80 | 6.70 | 0.49 | | | | | | |
| yPyAyPy | $S_6$ | $S_5$ ($B_{x1}$) | 2.71 | 2.90 | 17.72 | −19.07 | 1.26 | | | | | | |
| | | $S_{11}$ ($B_{x2}$) | 3.47 | 2.90 | 9.81 | 25.44 | 2.02 | 0.25 | 0.93 | −0.43 | 0.85 | 0.18 | −0.78 |
| | | $S_1$ ($Q_x$) | 2.01 | 2.90 | 8.70 | −9.41 | 0.56 | | | | | | |

[a] Listed are the INDO/MRDCI calculated excitation energies (eV) of 2PA-active and intermediate states and transition dipoles (Debye); if not specified, the component along the *x*-direction of the transition dipole moment is quoted. For dimers, we also give the relative participations of resulting 2PA channels for the dimers; channels involving $Q_x$ as intermediate state are denoted as QQ, channels with $B_{xi}$ ($i = 1,2$) intermediate state as $B_{xi}B_{xi}$ channels and mixed channels with $Q_x$, $B_{x1}$, or $B_{x2}$ as one of the intermediated states as $QB_{xi}$ and $B_{x1}B_{x2}$ channels, respectively.

ByPy). In the first two molecules, there come significant contributions from QQ channel(s). They are particularly enhanced in yPyyPy, in which they exceed 50% mostly to the cost of all $B_{xi}B_{xj}$-related channels ($i,j = 1,2$) caused by the much larger transition dipole moment $\mu_{ge}$ for the $Q_x$ state (with similar detuning energies for the $S_{26}$ state in PyyP and the $S_{21}$, $S_{23}$, and $S_{24}$ states in yPyyPy). The combined contribution of $QB_{xi}$ channels is at least 30% (up to 43% in $S_{21}$ of yPyyPy, compare to 40−49% in PyyP) and remains essential, even though it is somewhat diminished with respect to PyyP, whose $\mu_{ef}$ are larger than in yPyyPy. The larger number of 2PA active states in the relevant energy region in yPyyPy also results in some increase in $\sigma_2$. These aspects are responsible for the overall increase of the cross section in yPyyPy compared to PyyP. In yPyByPy, the Q-channel contributions are particularly small due to relatively large detuning energies and small $\mu_{ef}$. This cannot be fully compensated by B-channel contributions, among which we observe despite their large $\mu_{ge}$ and $\mu_{ef}$ a strong compensation of $B_{x1}$- and $B_{x2}$-based channels, resulting in a smaller overall cross section.

In the two nonplanar dimers PyP and yPyAyPy, the larger cross section in the latter molecule can be mainly explained by a low-lying $S_8$ state in which $|\mu_{ef}|$ from $B_{x2}$ is substantially smaller than its counterpart from $B_{x1}$; typically, as seen in all other cases listed in Table 2, $|\mu_{ef}|$ from $B_{x2}$ largely exceeds the one into $B_{x1}$. Therefore, $B_{x2}$-related channels do not compensate for the $B_{x1}$-based cross section, whose associated dipole moments are appreciably larger than in PyP due to the enhanced conjugation length. Additionally, also $\mu_{ge}$ for the Q-channel in yPyAyPy becomes larger than in PyP, being partly compensated by a larger detuning energy. The main conclusion from the above considerations is that, in the series of dimers, the actually calculated trends for cross sections strongly depend on a subtle interplay between the evolutions of transition dipoles (and for the Q-channels, which are much closer to a double-resonance situation, also the trends for the detuning energies). This makes a detailed analysis of the actual origin of the trends virtually impossible and also implies that the very details of the obtained trends can be significantly influenced by changing "external" parameters, like the molecular conformation (see above), or possibly also by using different computational methodologies.

**D. Three-Photon Absorption.** Figure 4 shows the *xxxxxx* components of the MRDCI/CV calculated 3PA spectrum of the investigated porphyrin derivatives. Considering that the *xxxxxx* component dominates the overall response, the expected cross section for an isotropic solution corresponds to $^1/_7$ of the values in Figure 4.[19a]

*i. yPy Monomer.* At this point, it should be mentioned that due to symmetry selection rules in centrosymmetric molecules, the one-photon allowed states are also 3PA active. For the monomer (yPy), there is thus a very weak 3PA peak for absorption into the $Q_x$ band at ca. 0.70 eV and a second, stronger 3PA into the $B_x$ band at ca. 1.07 eV (compare Table 1).

*ii. Porphyrin Dimers.* In the porphyrin dimers, 3PA into $Q_x$ band remains very weak; therefore, the corresponding energy range (photon energies below 0.7 eV) is not shown in Figure 4. In the region of the $B_x$ bands of the porphyrin dimers, there are two 3PA peaks; the lower-energy 3PA peak between 0.90 and 1.00 eV corresponds to excitation into the $B_{x1}$ state and the second (higher-energy 3PA peak between 1.15 and 1.25 eV) corresponds to excitation into $B_{x2}$. (At the high-energy limit of the plots, the onset of another strong peak is observed for several of the materials; at these energies, however, one approaches a triple resonance situation, which makes those states difficult to access experimentally. They will thus not be further discussed.) The 3PA cross section for excitation into $B_{x1}$ is increased by about 3 orders of magnitude compared to excitation into the $B_x$ state of the monomer. $\sigma_3$ for $B_{x2}$ is further increased by more than an 1 order of magnitude. The largest longitudinal component of $\sigma_3$ in the investigated energy range is found for yPyyPy

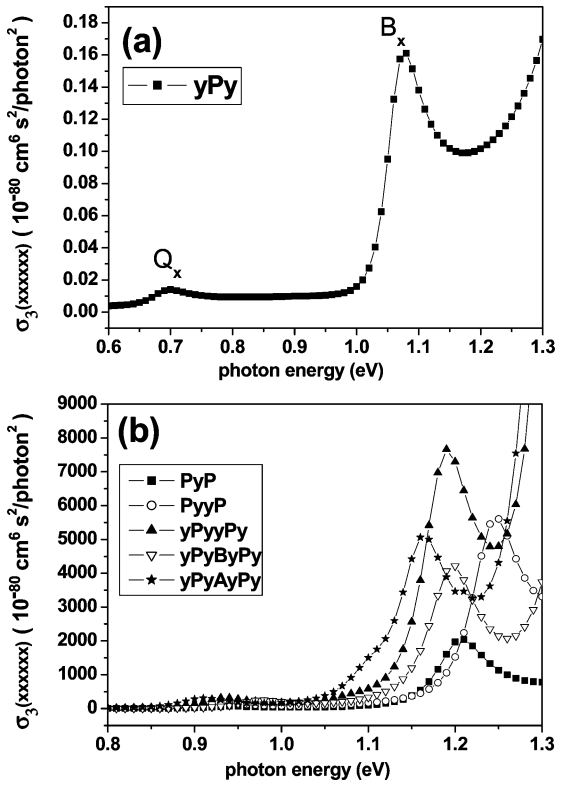


**Figure 4.** MRDCI/CV calculated *xxxxxx* component of the three-photon absorption spectra of (a) the monomer and (b) the dimers.

around 1.2 eV, corresponding to $7.0 \times 10^{-77}$ $cm^6$ $s^2$ (the averaged $\sigma_3$ is $1.0 \times 10^{-77}$ $cm^6$ $s^2$), which is comparable to that of an organometallic dendrimer ($\sigma_3 = 1.5 \times 10^{-77}$ $cm^6$ $s^2$) measured by Samoc et al. in very recent paper.[42]

For comparative reasons, we have again used a perturbative tensor-based approach (the T-tensor method[19,43]) to compute $\sigma_3$. $\sigma_3(\omega)$, when averaged over molecular orientations assuming an isotropic sample, can be written as (assuming linearly polarized light)

$$\sigma_3(\omega) = \frac{4\pi^3(\hbar\omega)^3 L^6}{3n^3c^3\hbar\cdot 35}\sum_f \left| 2\sum_{ijk} T^{ijk}_{g\to f} T^{ijk\ *}_{g\to f} + 3\sum_{ijk} T^{iij}_{g\to f} T^{kkj\ *}_{g\to f} \right| \left\{ \frac{\Gamma}{(E_{gf} - 3\hbar\omega)^2 + \Gamma^2} \right\} \quad (17)$$

where $c$ is the speed of light in vacuum, $L$ denotes a local-field correction, and $n$ the refractive index of the medium (both set to 1 for vacuum). $T_{g\to f}$ corresponds to the three-photon transition amplitude from the ground state to a final three-photon state $|f\rangle$, with tensor $ijk$ component defined as

$$T^{ijk}_{g\to f} = \sum P_{ijk} \sum_{m,n} \frac{\langle g|\mu_i|m\rangle\langle m|\mu_j|n\rangle\langle n|\mu_k|f\rangle}{(E_{gm} - \hbar\omega - i\Gamma)(E_{gn} - 2\hbar\omega - i\Gamma)} \quad (18)$$

where $P_{ijk}$ denotes a complete permutation of the indices $i$, $j$, and $k$, obtaining trends that are again consistent with the results of the CV method. Thus, we have been able to analyze the dominant channels contributing to $|T_{g\to f}|^2(E_{gf})^3\,\Gamma/\{(E_{gf} - 3\hbar\omega)^2 + \Gamma^2\}$ for 3PA into the high-energy main peak and the low-energy peak, in analogy to what is discussed above for 2PA. Here, the involved channels for 3PA into a particular final state $|f\rangle$ involve two intermediate states, and the magnitude of a certain channel is again determined by transition dipoles and detuning energies between the various states. Information on the mathematical details of few-state models for 3PA can for example be found in refs 19b,44.

The most relevant channels for 3PA into the $B_{x1}$ and $B_{x2}$ states can be found in Tables S10 and S11 in the Supporting Information. Here we have classified the channels depending on whether the first (one-photon allowed) intermediate state is the $Q_x$, the $B_{x1}$, or the $B_{x2}$ state; the second intermediate state is then one of the 2PA active states discussed above. In general, we find that B-channel contributions strongly dominate over Q-channel contributions. As far as the former are concerned, the contributions of $B_{x1}$ related channels, in the calculations, are typically larger than those involving $Bx_2$ states due to the larger calculated transition dipole moment between the ground state and $B_{x1}$.

## IV. Conclusions

To summarize, we have successfully implemented the correction vector method within MRDCI/ INDO to study the structure−properties relationships for 2PA and 3PA of covalently linked porphyrin dimers. The ground-state-based CV method is found to be fully consistent with approaches like the S-tensor approach for 2PA and the T-tensor approach for 3PA (or the SOS method) but avoids the difficulty to resolve excited states.

The calculated spectra and trends are in good agreement with experimental observations. In particular, we also find an increase of the 2PA cross section by about 2 orders of magnitude when going from the monomer yPy to the corresponding dimer yPyyPy. Also most experimental trends for dimers with different linking groups are well reproduced. The observed trends are analyzed on the basis of few-state models, where it turns out that including only the $Q_x$ state as an intermediate state (as done previously) is not sufficient. While the increase in the 2PA cross section when going from the monomer to the yPyyPy dimer can be clearly explained by the increase of $\mu_{ge}$ and much more importantly $\mu_{ef}$ and the decrease of the detuning energies ($E_{ge} - E_{ef}/2$), the observed evolution among the various dimers depends on a subtle interplay between various transition dipoles and detuning energies.

For 3PA, where the active states are in principle the same as for linear absorption, the cross section into the $Q_x$-band remains negligibly small. For the dimers, a now more than 3 orders of magnitude increase in the cross section is obtained for the $B_{x1}$ band compared to the B-band of the monomer, while the cross section into $B_{x2}$ is even another order of magnitude larger.

**Acknowledgment.** This work is supported by NSFC (grant nos. 10425420, 20433070, 20421101, 90503013) as well as the super computer center of the Chinese Academy of Sciences.

**Supporting Information Available:** Frontier Kohn−Sham orbitals of yPy monomer from the first-principles DFT calculations; quantum-chemical calculations (choice of the CI-active space and the reference determinants in the INDO/MRDCI procedure); transition energy and transition dipole moment in the $x,y$ direction for Q- and B-band of yPy, $Zn_1(T)_2$ and $Zn_1(TT)_2$ compounds; dominant channels that contribute to 3PA into the high-energy main peak and the low-energy peak. This material is available free of charge via the Internet at http://pubs.acs.org.

## References and Notes

(1) (a) He, G. S.; Xu, G. C.; Prasad, P. N.; Reinhardt, B. A.; Bhatt, J. C.; McKellar, R.; Dillard, A. G. *Opt. Lett.* **1995**, *20*, 435. (b) Ehrlich, J. E.;

Wu, X. L.; Lee, I.-Y. S.; Hu, Z.-Y.; Rochel, H.; Marder, S. R.; Perry, J. W. *Opt. Lett.* **1997**, *22*, 1843.

(2) (a) Maruo, S.; Nakamura, O.; Kawata, S. *Opt. Lett.* **1997**, *22*, 132. (b) Cumpston, B. H.; Ananthavel, S. P.; Barlow, S.; Dyer, D. L.; Ehrlich, J. E.; Erskine, L. L.; Heikal, A. A.; Kuebler, S. M.; Lee, I.-Y. S.; McCord-Maughon, D.; Qin, J.; Röckel, H.; Rumi, M.; Wu, X.-L.; Marder, S. R.; Perry, J. W. *Nature* **1999**, *398*, 51. (c) Kawata, S.; Sun, H.-B; Tanaka, T.; Takada, K. *Nature (London)* **2001**, *412*, 697. (d) Zhou, W. H.; Kuebler, S. M.; Braun, K. L.; Yu, T. Y.; Cammack, J. K.; Ober, C. K.; Perry, J. W.; Marder, S. R. *Science* **2002**, *296*, 1106.

(3) (a) Parthenopoulos, D. A.; Rentzepis, P. M. *Science* **1989**, *245*, 843. (b) Strickler, J. H.; Webb, W. W. *Opt. Lett.* **1991**, *16*, 1780. (c) Dvornikov, A. S.; Rentzepis, P. M. *Opt. Commun.* **1995**, *119*, 341. (d) Belfield, K. D.; Schafer, K. J. *Chem. Mater.* **2002**, *14*, 3656.

(4) Ogawa, K.; Ohashi, A.; Kobuke, Y.; Kamada, K.; Ohta, K. *J. Am. Chem. Soc.* **2003**, *125*, 13356.

(5) Kim, D. Y.; Ahn, T. K.; Kwon, J. H.; Kim, D.; Ikeue, T.; Aratani, A.; Osuka, A.; Shigeiwa, M.; Maeda, S. *J. Phys. Chem. A* **2005**, *109*, 2996.

(6) Inokuma, Y.; Ono, N.; Uno, H.; Kim, D. Y.; Nob, S. B.; Kim, D.; Osuka, A. *Chem. Commun.* **2005**, 3702.

(7) Collini, E.; Ferrante, C.; Bozio, R. *J. Phys. Chem. B* **2005**, *109*, 2.

(8) Ahn, T. K.; Kim, K. S.; Kim, D. Y.; Noh, S. B.; Aratani, N.; Ikeda, C.; Osuka, A.; Kim, D. *J. Am. Chem. Soc.* **2006**, *128*, 1700.

(9) Drobizhev, M.; Meng, F.; Rebane, A.; Stepanenko, Y.; Nickel, E.; Spangler, C. W. *J. Phys. Chem. B* **2006**, *110*, 9802.

(10) Drobizhev, M.; Stepanenko, Y.; Rebane, A.; Wilson, C. J.; Screen, T. E. O.; Anderson, H. L. *J. Am. Chem. Soc.* **2006**, *128*, 12432.

(11) Humphrey, J. L.; Kuciauskas, D. *J. Am. Chem. Soc.* **2006**, *128*, 3902.

(12) Misra, R.; Kumar, R.; Chandrashekar, T. K.; Nag, A.; Goswami, D. *Org. Lett.* **2006**, *8*, 629.

(13) (a) Bonnett, R. *Chem. Soc. Rev.* **1995**, *24*, 19. (b) Prasad, P. N. *Introduction to Biophotonics*; Wiley-Interscience: Hoboken, NJ, 2003; Chapter 12.

(14) Remn, A.; Wild, U. P.; Rebane, A. *J. Phys. Chem. A* **2002**, *106*, 3045.

(15) (a) Drobizhev, M.; Stepanenko, Y.; Dzenis, Y.; Karotki, A.; Rebane, A.; Taylor, P. N.; Anderson, H. L. *J. Am. Chem. Soc.* **2004**, *126*, 15352. (b) Drobizhev, M.; Stepanenko, Y.; Dzenis, Y.; Karotki, A.; Rebane, A.; Taylor, P. N.; Anderson, H. L. *J. Phys. Chem. B* **2005**, *109*, 7223.

(16) (a) Orr, B. J.; Ward, J. F. *Mol. Phys.* **1971**, *20*, 513. (b) Pati, S. K.; Marks, T. J.; Rater, M. A. *J. Am. Chem. Soc.* **2001**, *123*, 7287.

(17) (a) Olsen, J.; Jørgensen, P. *J. Chem. Phys.* **1985**, *82*, 3235. (b) Koch, H.; Jørgensen, P. *J. Chem. Phys.* **1990**, *93*, 3333. (c) Helgaker, T.; Jensen, H. J. Aa.; Jørgensen, P.; Olsen, J.; Ruud, K.; Ågren, H.; Auer, A. A.; Bak, K. L.; Bakken, V.; Christiansen, O.; Coriani, S.; Dahle, P.; Dalskov, E. K.; Enevoldsen, T.; Fernandez, B.; Hättig, C.; Hald, K.; Halkier, A.; Heiberg, H.; Hettema, H.; Jonsson, D.; Kirpekar, S.; Kobayashi, R.; Koch, H.; Mikkelsen, K. V.; Norman, P.; Packer, M. J.; Pedersen, T. B.; Ruden, T. A.; Sanchez, A.; Saue, T.; Sauer, S. P. A.; Schimmelpfenning, B.; Sylvester-Hvid, K. O.; Taylor, P. R.; Vahtras, O. *DALTON*, an ab initio electronic structure program, release 1.2; 2001; available from http://www.kjemi.uio.no/software/dalton /dalton.html. (d) Christiansen, O.; Jørgensen, P.; Hättig, C. *Int. J. Quantum Chem.* **1998**, *68*, 1. (e) Christiansen, O.; Gauss, J.; Stanton, J. F. *Chem. Phys. Lett.* **1998**, *292*, 437. (f) Gauss, J.; Christiansen, O.; Stanton, J. F. *Chem. Phys. Lett.* **1998**, *296*, 117. (g) Christiansen, O.; Gauss, J.; Stanton, J. F. *Chem. Phys. Lett.* **1999**, *305*, 147.

(18) Soos, Z. G.; Ramasesha, S. *J. Chem. Phys.* **1989**, *90*, 1067.

(19) (a) Cronstrand, P.; Luo, Y.; Norman, P.; Ågren, H. *Chem. Phys. Lett.* **2003**, *375*, 233. (b) Cronstrand, P.; Luo, Y.; Ågren, H. *J. Chem. Phys.* **2004**, *121*, 2020.

(20) (a) Day, P. N.; Nguyen, K. A.; Pachter, R. *J. Phys. Chem. B* **2005**, *109*, 1803. (b) Day, P. N.; Nguyen, K. A.; Pachter, *J. Chem. Phys.* 2006, *125*, 094103.

(21) (a) Masunov, A.; Tretiak, S. *J. Phys. Chem. B* **2004**, *108*, 899. (b) Badaeva, E. A.; Timofeeva, T. V.; Masunov, A.; Tretiak, S. *J. Phys. Chem. A* **2005**, *109*, 7276.

(22) Dreuw, A.; Head-Gordon, M. *Chem. Rev.* **2005**, *105*, 4009.

(23) (a) Ramasesha, S.; Soos, Z. G. *Chem. Phys. Lett.* **1988**, *153*, 171. (b) Ramasesha, S.; Shuai, Z.; Brédas, J. L. *Chem. Phys. Lett.* **1995**, *245*, 224. (c) Shuai, Z.; Ramasesha, S.; Brédas, J. L. *Chem. Phys. Lett.* **1996**, *250*, 14.

(24) Yi, Y. P; Zhu, L. Y.; Shuai, Z. G. *J. Chem. Phys.* **2006**, *125*, 164505.

(25) Frisch, M. J.; Trucks, G. W.; Schlegel, H. B.; Scuseria, G. E.; Robb, M. A.; Cheeseman, J. R.; Montgomery, J. A., Jr.; Vreven, T.; Kudin, K. N.; Burant, J. C.; Millam, J. M.; Iyengar, S. S.; Tomasi, J.; Barone, V.; Mennucci, B.; Cossi, M.; Scalmani, G.; Rega, N.; Petersson, G. A.; Nakatsuji, H.; Hada, M.; Ehara, M.; Toyota, K.; Fukuda, R.; Hasegawa, J.; Ishida, M.; Nakajima, T.; Honda, Y.; Kitao, O.; Nakai, H.; Klene, M.; Li, X.; Knox, J. E.; Hratchian, H. P.; Cross, J. B.; Bakken, V.; Adamo, C.; Jaramillo, J.; Gomperts, R.; Stratmann, R. E.; Yazyev, O.; Austin, A. J.; Cammi, R.; Pomelli, C.; Ochterski, J. W.; Ayala, P. Y.; Morokuma, K.; Voth, G. A.; Salvador, P.; Dannenberg, J. J.; Zakrzewski, V. G.; Dapprich, S.; Daniels, A. D.; Strain, M. C.; Farkas, O.; Malick, D. K.; Rabuck, A. D.; Raghavachari, K.; Foresman, J. B.; Ortiz, J. V.; Cui, Q.; Baboul, A. G.; Clifford, S.; Cioslowski, J.; Stefanov, B. B.; Liu, G.; Liashenko, A.; Piskorz, P.; Komaromi, I.; Martin, R. L.; Fox, D. J.; Keith, T.; Al-Laham, M. A.; Peng, C. Y.; Nanayakkara, A.; Challacombe, M.; Gill, P. M. W.; Johnson, B.; Chen, W.; Wong, M. W.; Gonzalez, C.; Pople, J. A. *Gaussian 03*, Gaussian, Inc.: Pittsburgh, PA, 2003.

(26) Buenker, R. J.; Peyerimhoff, S. D. *Theor. Chim. Acta* **1974**, *35*, 33.

(27) (a) Pople, J. A.; Beveridge, D. L.; Dobosh, P. A. *J. Chem. Phys.* **1967**, *47*, 2026. (b) Ridley, J.; Zerner, M. *Theor. Chim. Acta* **1973**, *32*, 111.

(28) Mataga, N.; Nishimoto, K. *Z. Phys. Chem. (Munich)* **1957**, *13*, 140.

(29) Liu, X. J.; Feng, J. K.; Ren, A. M.; Cheng, H.; Zhou, X. *J. Chem. Phys.* **2004**, *120*, 11493.

(30) Zojer, E.; Beljonne, D.; Kogej, T.; Vogel, H.; Marder, S. R.; Perry, J. L.; Brédas, J. L. *J. Chem. Phys.* **2002**, *116*, 3646.

(31) (a) Rubtsov, I .V.; Susumu, K.; Rubstov, G. I.; Therien, M. J. *J. Am. Chem. Soc.* **2003**, *125*, 2687. (b) Kumble, R.; Palese, S.; Lin, V. S.-Y.; Therien, M. J.; Hochstrasser, R. M. *J. Am. Chem. Soc.* **1998**, *120*, 11489.

(32) Muranaka, A.; Asano, Y.; Tsuda, A.; Osuka, A.; Kobayashi, N. *Chem. Phys. Chem.* **2006**, *7*, 1235.

(33) (a) Taylor, P. N.; Huuskonen, J.; Rumbles, G.; Aplin, R. T.; Williams, R.; Anderson, H. L. *Chem. Commun.* **1998**, 909. (b) Aenold, D. P.; James, D. A.; Kennard, C. H. L.; Smith, G. *J. Chem. Soc., Chem. Commun.* **1994**, 2131.

(34) Chung, S.; Zheng, S.; Odani, T.; Beverina, L.; Fu, J.; Padilha, L. A.; Biesso, A.; Hales, J. M.; Zhan, X. W.; Schmidt, K.; Ye, A. J.; Zojer, E.; Barlow, S.; Hagan, D. J.; Van Stryland, E. W.; Yi, Y. P.; Shuai, Z. G.; Pagani, G. A.; Brédas, J. L.; Perry, J. W.; Marder, S. R. *J. Am. Chem. Soc.* **2006**, *128*, 14444.

(35) Beljonne, D.; O'Keefe, G. E.; Hamer, P. J.; Friend, R. H.; Anderson, H. L.; Brédas, J. L. *J. Chem. Phys.* **1997**, *106*, 9439.

(36) For the latter two molecules, the actual maxima of the features are not well resolved in the experiments, but photon/state energies for the highest energy data points imply that one is at least very close to the maxima of the calculations.

(37) We had done a test for PyyP dimer by rotating the two porphyrin rings to about 40°. DFT based single-point energy calculations show that the energy barrier between the twisted and the planar PyyP dimer is 3.69 kcal/mol. At the same time, the calculated 2PA cross section peak value of the twisted PyyP dimer is significantly reduced from 19195 GM to 4536 GM.

(38) (a) Rumi, M.; Ehrlich, J. E.; Heikal, A. A.; Perry, J. W.; Barlow, S.; Hu, Z.; McCord-Maughon, D.; Parker, T. C.; Röckel, H.; Thayumanavan, S.; Marder, S. R.; Beljonne, D.; Brédas, J. L. *J. Am. Chem. Soc.* **2000**, *122*, 9500. (b) Dirk, C. W.; Cheng, L. T.; Kuzyk, M. G. *Int. J. Quantum Chem.* **1992**, *43*, 27. (c) Mazumdar, S.; Duo, D.; Dixit, S. N. *Synth. Met.* **1993**, *57*, 3881. (d) Albota, M.; Beljonne, D.; Brédas, J. L.; Ehrlich, J. E.; Fu, J.-Y.; Heikal, A. A; Hess, S. E.; Kogej, T.; Levin, M. D.; Marder, S. R.; McCord-Maughon, D.; Perry, J. W.; Röckel, H.; Rumi, M.; Subramaniam, G.; Webb, W. W.; Wu, X.-L.; Xu, C. *Science* **1998**, *281*, 1653. (e) Cronstrand, P.; Luo, Y.; Agren, H. *Chem. Phys. Lett.* **2002**, *352*, 262. (f) Zojer, E.; Beljonne, D.; Pacher, P.; Brédas, J. L. *Chem.—Eur. J.* **2004**, *10*, 2668. (h) Blanchard-Desce, M.; Barzoukas, M. *J. Opt. Soc. Am. B* **1998**, *15*, 302.

(39) Luo. Y.; Norman, P.; Macak, P.; Agren, H. *J. Phys. Chem. A* **2000**, *104*, 4718.

(40) Anderson, R. J.; Holtom, G. R.; McClain, W. M. *J. Chem. Phys.* **1979**, *70*, 4310.

(41) Zojer, E.; Wenseleers, W.; Pacher, P.; Barlow, S.; Halik, M.; Grasso, C.; Perry, J. W.; Marder, S. R.; Brédas, J.-L. *J. Phys. Chem. B* **2004**, *108*, 8641.

(42) Samoc, M.; Morrall, J. P.; Dalton, G. T.; Cifuentes, M. P.; Humphrey, M. G. *Angew. Chem., Int. Ed.* **2007**, *46*, 731.

(43) Zhu, L.; Yang, X.; Yi, Y.; Xuan, P.; Shuai, Z.; Chen, D.; Zojer, E.; Brédas, J. L.; Beljonne, D. *J. Chem. Phys.* **2004**, *121*, 11060.

(44) Zhu, L.; Yi, Y.; Shuai, Z.; Brédas, J. L.; Beljonne, D.; Zojer, E. *J. Chem. Phys.* **2006**, *125*, 044101.